AGU100 ADVANCING EARTH AND SPACE SCIENCE

JGR

Journal of Geophysical Research: Oceans

RESEARCH ARTICLE
10.1029/2018JC014264

Key Points:
- The Mauritania Current exhibits pronounced seasonal variability both at the surface and at depth
- Seasonal strengthening of the Mauritania Current in boreal spring is linked to variability in local wind stress curl
- Boundary circulation seasonality impacts the local water mass distribution and ventilation of the lower central water layer

Correspondence to:
T. Klenz,
tklenz2@alaska.edu

Citation:
Klenz, T., Dengler, M., & Brandt, P. (2018). Seasonal variability of the Mauritania Current and hydrography at 18°N. *Journal of Geophysical Research: Oceans*, *123*. https://doi.org/10.1029/2018JC014264

Received 12 JUN 2018
Accepted 22 OCT 2018
Accepted article online 24 OCT 2018

Seasonal Variability of the Mauritania Current and Hydrography at 18°N

T. Klenz[1,2], M. Dengler[1], and P. Brandt[1,3]

[1]GEOMAR Helmholtz Centre for Ocean Research Kiel, Kiel, Germany, [2]Now at College of Fisheries and Ocean Sciences, University of Alaska Fairbanks, Fairbanks, AK, USA, [3]Faculty of Mathematics and Natural Sciences, Kiel University, Kiel, Germany

Abstract Extensive field campaigns in the Mauritanian upwelling region between 2005 and 2016 provide the database for analyzing the seasonal variability of the eastern boundary circulation (EBC) and associated water mass distribution at 18°N. The data set includes shipboard upper ocean current, hydrographic, and oxygen measurements from nine research cruises conducted during upwelling (December to April) and relaxation (May to July) seasons. During the upwelling season, the EBC closely resembles a classical eastern boundary current regime, with a poleward undercurrent flowing beneath an equatorward coastal jet. In contrast, elevated poleward flow exceeding 30 cm/s and extending from the surface down to 250-m depth is observed during the relaxation season. The pronounced seasonal variability of the across-shore structure of the EBC can be related to local wind forcing and is in general agreement with Sverdrup balance. The EBC transport is correlated to the wind stress curl leading the transport by 7 days. The short lead time suggests a fast response of locally forced waves adjusting the EBC to wind forcing. The seasonal and vertical water mass distribution is presented based on hydrographic observations. The meridional oxygen distribution and corresponding water mass partitioning into South and North Atlantic Central Water masses reveal a possible northerly ventilation pathway in the deeper layers of the central water stratum. Our results suggest that the poleward surface flow and the poleward undercurrent both are a consequence of the cyclonic wind stress curl forcing and thus propose to name it the Mauritania Current.

Plain Language Summary In this study we use a multiyear data set of shipboard current measurements from nine research cruises conducted between 2005 and 2016. We provide a description of the boundary circulation and its seasonality in the Mauritanian upwelling region off Northwest Africa, which is poorly understood owing to the lack of sufficient observations so far. We find poleward flow in the Mauritania Current to be enhanced and extending from the surface to about 250-m depth during the relaxation season between May and July. During the upwelling season between December and April, weaker poleward flow is confined to the subsurface layers while equatorward flow dominates at the surface. We relate the observed seasonal variability to local wind forcing and find general agreement with theoretical considerations. Water masses in the Mauritanian upwelling region are of both North and South Atlantic origin. Using measurements of temperature and salinity, we present the seasonal and vertical water mass distribution in relation to the boundary circulation. Meridional oxygen and water mass distributions reveal a possible ventilation pathway for oxygenated waters from the north between 250- and 500-m depth.

1. Introduction

The Canary upwelling system in the eastern tropical North Atlantic (ETNA; Table 1) is among the four major eastern boundary coastal upwelling systems in the world oceans together with the Peruvian (e.g., Brink et al., 1983) and Californian (e.g., Marchesiello et al., 2003) upwelling systems in the tropical South and North Pacific, respectively, and the Benguela upwelling system in the tropical South Atlantic (e.g., Mohrholz et al., 2014). As part of the Canary upwelling, the Mauritanian upwelling region (MUR; Figure 1) exhibits a pronounced seasonality (e.g., Lathuilière et al., 2008; Mittelstaedt, 1983; Van Camp et al., 1991). Upwelling-favorable winds in the MUR are largely controlled by the seasonal migration of the intertropical convergence zone, and the main upwelling season lasts from December to April (Barton et al., 1998; Brandt et al., 2015; Mittelstaedt, 1983, 1991). During this period, the MUR exhibits elevated biological productivity in the surface layer due to the supply of cold, nutrient-rich waters of predominantly South Atlantic origin to the continental slope and shelf region (Mittelstaedt, 1983, 1991; Peña-Izquierdo et al., 2015).

Table 1
Frequently Used Abbreviations in This Paper

Abbreviation	Meaning
AAIW	Antarctic Intermediate Water
ADCP	Acoustic Doppler current profiler
CTWs	Coastally trapped waves
EBC	Eastern boundary circulation
ETNA	Eastern tropical North Atlantic
MC	Mauritania Current
MUR	Mauritanian upwelling region
NACW/SACW	North/South Atlantic Central Water
NECC	North Equatorial Countercurrent
NEUC	North Equatorial Undercurrent
PUC	Poleward undercurrent
TSW	Tropical Surface Water
uCW/lCW	Upper/lower Central Water

The main upwelling season is followed by a relaxation season (Lathuilière et al., 2008), in which the trade winds weaken and surface flow is predominantly poleward (Mittelstaedt, 1991). Geostrophic surface velocities (Figure 1) derived from satellite altimetry show poleward velocities within 200 km of the coast in the MUR up to 20°N during May to July, while during the upwelling season, equatorward velocities prevail (Figure 1). The countercurrent, flowing against the equatorward winds during the relaxation season, is generally referred to as the Mauritania Current (MC). Together with the poleward undercurrent (PUC; Barton, 1989), it comprises the eastern boundary circulation (EBC) in the MUR.

Previous observational efforts studying the EBC in the MUR have been limited to single cruise observations or short-term mooring programs, and very little is known about its seasonal variability. The PUC is usually observed attached to the continental slope between 50- and 300-m depth having a width of 30–60 km (Barton, 1989; Mittelstaedt, 1983; Peña-Izquierdo et al., 2012). Maximum poleward velocity is observed to exceed 0.2 m/s (Peña-Izquierdo et al., 2012). The MC is often described as indistinguishable from or as the surface manifestation of the PUC (Mittelstaedt, 1983; Peña-Izquierdo et al., 2012).

The dynamics of eastern boundary upwelling systems have been studied through a variety of theoretical and modeling approaches for various regional settings (e.g., Fennel, 1999; Fennel et al., 2012; Kounta et al., 2018; McCreary et al., 1987; McCreary & Chao, 1985; Philander & Yoon, 1982). McCreary and Chao (1985) using a linear general circulation model showed that a PUC, set up by coastally trapped waves (CTWs) due to the sudden onset of wind forcing (Philander & Yoon, 1982), only matched those typically observed in the California current system when a local wind stress curl was introduced. Marchesiello et al. (2003) compared eastern boundary upper ocean transports from simulations of the California Current system using different regional

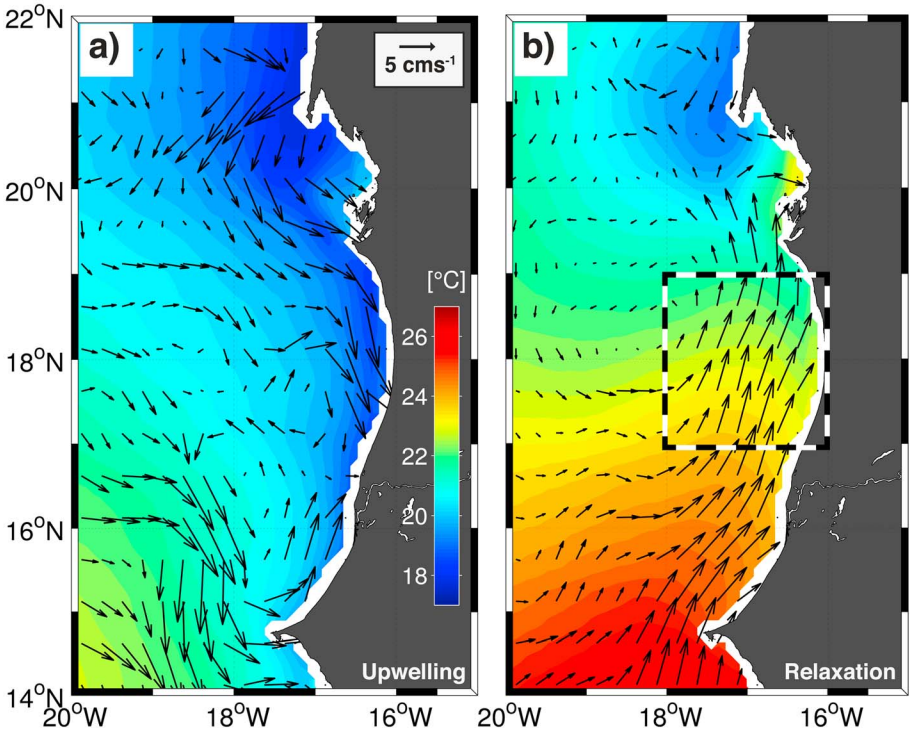

Figure 1. Mean microwave optimally interpolated sea surface temperature (color contours; http://www.remss.com) and geostrophic surface velocities (arrows) from absolute dynamic topography measurements (http://marine.copernicus.eu/) for (a) January to March (upwelling season) and (b) May to July (relaxation season) in the Mauritanian upwelling region. The study region is highlighted by the square in (b).

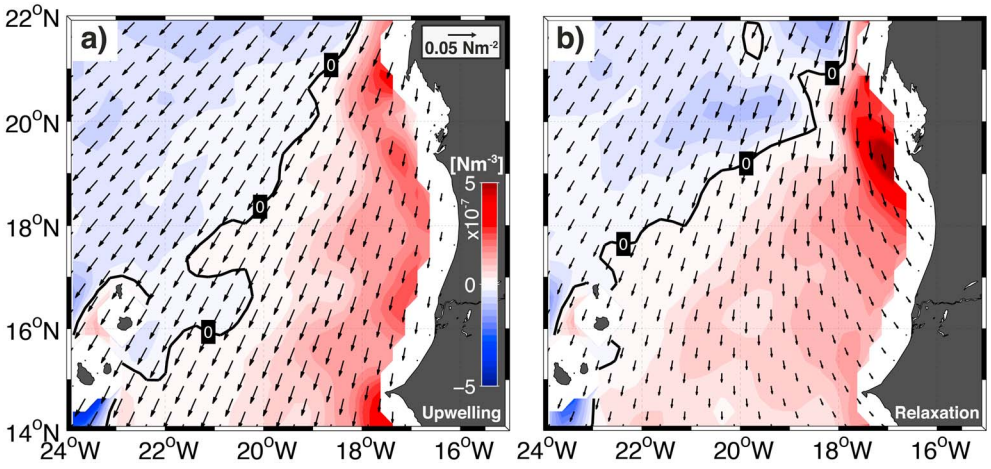

Figure 2. Climatological wind stress (arrows) and wind stress curl (color contours) from the Scatterometer Climatology of Ocean Winds (Risien & Chelton, 2008) for (a) January to March (upwelling season) and (b) May to July (relaxation season). The contour line of zero wind stress curl (i.e., maximum wind stress) is shown in black.

ocean model simulation (ROMS) configurations with the Sverdrup transport determined from local wind stress curl. They found the model and Sverdrup transports at the eastern boundary to be quantitatively similar throughout the different latitudes investigated although the model flow was somewhat stronger. They confirmed that the poleward flow is predominately driven by the wind stress curl as had been previously suggested by Munk (1950) and McCreary et al. (1987). The somewhat stronger alongshore transport was attributed to eddy momentum fluxes (Reynolds stresses) that lead to increased poleward transport within a few tens of kilometers away from the coast.

McCreary et al. (1987) pointed out that equatorward surface flow in the coastal jet can exceed the poleward flow in a region of positive wind stress curl. More recently, Fennel et al. (2012) using an analytical model on an *f*-plane refined this view by showing that the distance of the wind stress maximum from the coast and hence the zonal structure of the wind stress curl is crucial for setting the near-surface flow structure of the EBC. Poleward flow forced by cyclonic wind stress curl was found to exceed equatorward flow within the coastal jet region with increasing distance of the wind stress maximum from the coast. In their solutions for the Benguela upwelling region, the EBC was characterized by a surfacing PUC flowing against the local, equatorward winds. Junker et al. (2015) extended the analytical model of Fennel et al. (2012) and used a regional model to show that on seasonal timescales, the meridional transport within the eastern boundary current varies in correspondence to the wind stress curl. However, to our knowledge and as pointed out by an anonymous reviewer, a general theory describing the EBC in upwelling regions on the beta-plane remains to be developed.

Cyclonic wind stress curl in the MUR persists throughout the year, with the distance of the wind maximum from the coast increasing from 400 km during the upwelling season to 600 km during the relaxation season (Figure 2). As suggested from satellite altimetry and in agreement with the analytical model of Fennel et al. (2012), the geostrophic surface flow close to the coast is in the direction of the local winds during the upwelling season (Figure 1), while it is poleward during the relaxation season when Ekman convergence occurs further offshore (Figures 1 and 2).

A significant influence of equatorially forced CTWs on the seasonality of the Mauritanian EBC as found, for example, for the Angolan (Kopte et al., 2018; Tchipalanga et al., 2018) EBC has not been reported. Polo et al. (2008) showed that signals of intraseasonal coastal Kelvin waves forced at the equator to extend to latitudes less than 15°N, only. In a recent elaborate analysis of an eddy-permitting ROMS, Kounta et al. (2018) found signatures of CTWs propagating poleward along the West African eastern boundary from 5°S to perhaps as far as 20°S during boreal fall and to a lesser extent during boreal spring. In their simulations, these waves were generated due to semiannual along-shore wind stress variability in the Gulf of Guinea. On their northward passage, energy of the CTWs is scattered into Rossby waves propagating westward. Both forms of variability were found to significantly contribute to EBC variability between 8°N and 15°N, particularly during boreal fall.

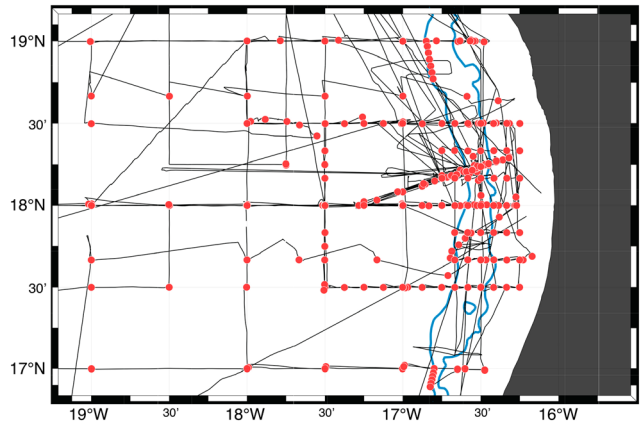

Figure 3. Cruise tracks (black lines) and conductivity-temperature-depth-oxygen stations (red dots) of nine research cruises (Table 2) conducted in the eastern tropical North Atlantic between 2005 and 2016 and used in this study. The 100- and 500-m isobaths are shown in blue. See Figure 1 for an overview of the regional setting of the study area.

Main water masses encountered in the MUR are the Tropical Surface Water (TSW), the North and South Atlantic Central Waters (NACW and SACW), and the Antarctic Intermediate Water (AAIW; Stramma et al., 2005). The main focus of this study will be on the central water stratum. The water mass distribution and renewal in the MUR is strongly influenced by the EBC. Low-salinity, nutrient-rich and cold central waters of South Atlantic origin are transported into the MUR by the northward boundary currents (Brandt et al., 2015; Glessmer et al., 2009; Peña-Izquierdo et al., 2012; Stramma et al., 2008; Voituriez & Chuchla, 1978). Thus, the seasonality in the EBC likely has a strong influence on the hydrography and water mass characteristics in the MUR as well as on the advective oxygen supply toward the continental slope and onto the shelf in the study area.

The main objective of the present study is to describe the seasonality of the boundary circulation, associated water mass changes in the central water stratum of the MUR, and its connection to the seasonal variability of the wind stress curl and associated Sverdrup dynamics. A comprehensive observational data set based on nine cruises conducted over a period of 11 years in the MUR is used to describe the seasonality of the EBC, water masses, and oxygen content in this sparsely studied part of the ETNA.

This paper is organized as follows. The data sets and methods employed for analysis are described in section 2, followed by a presentation of the results in section 3. Lastly, a general discussion and a conclusion are given in sections 4 and 5, respectively.

2. Data and Methods

2.1. Shipboard Data

Main basis for analysis in this study is an extensive data set of hydrographic and acoustic Doppler current measurements from nine research cruises performed in the ETNA (Figure 3) between March 2005 and August 2016 (Table 2). Altogether, 593 conductivity-temperature-depth-oxygen (CTD-O_2) profiles were available from the cruises. Upper ocean velocities in the water column during the individual cruises were measured by Ocean Surveyor 75-kHz vessel-mounted acoustic Doppler current profilers (vmADCPs) installed on the different research vessels. Estimates of zonal and meridional velocities (u and v, respectively) were available down to water depths of 700 m in 8-m bins. The uppermost reliable ADCP measurements varied between the individual vessels but were generally around 20-m water depth. Zonal and meridional velocities were rotated locally into alongshore and cross-shore components. Hydrographic and rotated velocity data from 17°N to 19°N were sorted according to local water depth and finally interpolated onto a reference topography resembling that along 18°N to derive mean sections for each cruise.

Table 2
Data From These Research Cruises Performed in the Eastern Tropical North Atlantic is Used

Cruise Short	Vessel	Date	Cruise report	CTD-O_2 profiles
P320	RV *Poseidon*	Mar–Apr 2005	Ruhland et al. (2005)	43[a]
M68/3	RV *Meteor*	Jul–Aug 2006	Koschinsky et al. (2009)	95
P347	RV *Poseidon*	Jan–Feb 2007	Dengler et al. (2008)	126
P348	RV *Poseidon*	Feb 2007	Bange (2008)	33
ATA3	RV *L'Atalante*	Feb 2008	Körtzinger (2008)	61
P399	RV *Poseidon*	Jun 2009	Bange (2011)	25
MSM17/4	RV *Maria S. Merian*	Mar–Apr 2011	Pfannkuche (2014)	69
M107	RV *Meteor*	Jun 2014	Sommer et al. (2015)	73
M129	RV *Meteor*	Aug 2016	Ekau et al. (2016)	68
				Σ 593

Note. References to the individual cruise reports are given. CTD-O_2 = conductivity-temperature-depth-oxygen.
[a]No O_2 data available.

For a description of the seasonal variability of hydrography and EBC, cruises were separated into two mean seasons. Following Lathuilière et al. (2008), cruises P320, P347, P348, ATA3, and MSM17/4 fall into the upwelling season from December to April, while cruises M68/3, P399, and M107 fall into the relaxation season from May to July. Cruise M129 was conducted toward the end of the relaxation season and was therefore excluded from either seasonal mean section.

Volume transports in the near-shore region were calculated in Sverdrup ([Sv] = 10^6 m^3/s) by integrating the alongshore velocity of the mean sections from the coast to 60 km offshore of the 100 m isobath (the depth of the shelf break). Different depth intervals were chosen based on water mass boundaries to be introduced in section 2.3. First, in order to describe the opposing flows observed at different depths, transports in the upper 20–250 m and between 250 and 500 m were calculated separately. Second, for a comparison with Sverdrup transport calculated from wind stress curl, the transport was calculated from 20 to 500 m.

2.2. Auxiliary Data

Here we used 10-m QuickSCAT winds for the period from January 2005 to November 2009, when the satellite mission ended, and 10 m ASCAT winds from 2007 to September 2016. Both products were downloaded from www.remss.com as weekly averages at 1/4° spatial resolution. Wind stress was estimated following Large and Pond (1981), from which the wind stress curl was calculated. We further made use of the Scatterometer Climatology of Ocean Winds, based on 122 months of QuickSCAT data (Risien & Chelton, 2008).

Absolute geostrophic sea surface velocities derived from absolute dynamic topography measurements are distributed by the E.U. Copernicus Marine Service Information (http://marine.copernicus.eu/). The product was downloaded for the observation period 2005–2016 at 1/4° resolution to supplement the vmADCP data in the surface layer.

Microwave optimally interpolated sea surface temperature (SST) radiometer data were obtained from www.remss.com. The downloaded product combines all available microwave radiometer SST measurements from a given day and was available at a gridded 9-km horizontal daily resolution.

2.3. Water Mass Analysis

Available hydrographic data from CTD measurements within the central water stratum in the study region (Figure 3) were analyzed for relative contributions of central waters of South and North Atlantic origin on respective isopycnal surfaces. This method aids in describing the central water mass distribution at the continental slope during the individual cruises and its connection to seasonal EBC variability. The linear potential temperature-salinity (θ-S) relationship of the SACW and NACW allowed for a composition analysis of individual water parcels (e.g., Johns et al., 2003; Peña-Izquierdo et al., 2012, 2015). Lower and upper potential density bounds used are 25.8 and 27.1 kg/m^3 (Stramma et al., 2005), further divided by the 26.8-kg/m^3 isopycnal into a lower Central Water (lCW) and upper Central Water (uCW; e.g., Elmoussaoui et al., 2005; Fischer et al., 2013; Peña-Izquierdo et al., 2012, 2015). We chose linear θ-S relationships for SACW and NACW source waters that represented a best fit to the observed data. Lower and upper salinity bounds were chosen to be between 35.1 and 35.65 for SACW and 35.37 and 37 for NACW. Potential temperature bounds were 9.6 and 17.9 °C for SACW and 10.8 and 21.8 °C for NACW. Following Johns et al. (2003), relative contributions of SACW and NACW were calculated from $\mathrm{SACW}\% = \frac{S_{\mathrm{NACW}} - S}{S_{\mathrm{NACW}} - S_{\mathrm{SACW}}} \times 100$ and NADW% = 100 − SACW%, where S denotes the salinity of the water sample and the subscripts denote the salinities of SACW and NACW source waters at the water sample density. It should be emphasized that water mass concentrations calculated using this method are to be seen as relative contributions to a given water sample and certainly depend on salinity and potential temperature bounds chosen for this analysis.

3. Results

3.1. Alongshore Flow and Transport

Poleward flow dominated over the continental slope and in the vicinity of the shelf break in the TSW and uCW layers during most cruises analyzed in this study (Figure 4). Noticeably enhanced poleward velocities were observed during the relaxation season, with current velocities exceeding 40 cm/s (e.g., in July 2006 and June 2009) above 100–150-m water depth (Figure 4). During July 2006, poleward flow was attached to the slope and across the continental shelf, with strongest velocities just above the shelf break. During June

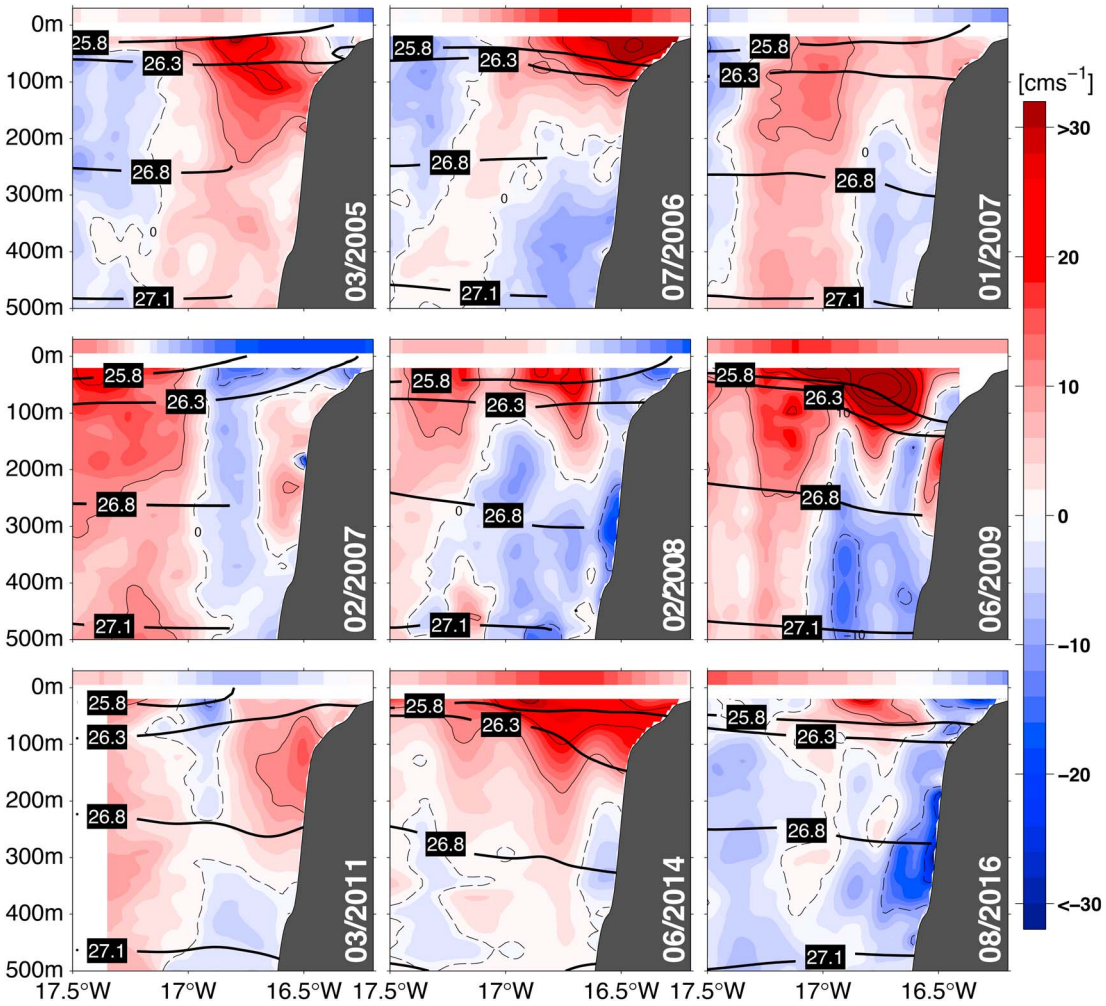

Figure 4. Alongshore velocities (cm/s, positive poleward) as a function of longitude and depth at 18°N between 2005 and 2016. Thick black contours depict potential density surfaces. The 26.8 kg/m^3 isopycnal separates the uCW from the lCW. Geostrophic surface velocities from altimetry averaged over the respective cruise period are indicated at the top of each panel.

2009 the strongest flow was confined to a shallow core at water depths above 100 m detached from the slope. Poleward flow during June 2014 extended over the entire shelf encompassing most of the uCW and parts of the lCW layer. The weak poleward flow component in the uCW layer during August 2016 differed from flow conditions observed during other cruises during the relaxation season. Here the flow was confined to the surface layer and was detached from the slope with equatorward velocities shoreward of the shelf break.

Equatorward flow dominated the shelf region during the upwelling season. This was most pronounced during February 2008 when equatorward velocities above 10 cm/s were observed. Poleward velocities were generally weaker than observed during the relaxation season, with maximum velocities around 10–15 cm/s near the continental slope.

Contrary to the relaxation season, the core of poleward flow was located between 100- and 200-m water depth during the upwelling season and was clearly separated from the surface. This separation from the surface was associated with a prevailing equatorward flow in the surface layer, which is indicated by the geostrophic surface velocities (Figure 1 and colorbars at the top of the panels in Figure 4). Together with the shallowing of the isopycnals toward the shore, this equatorward jet is the geostrophic response to the Ekman divergence close to the coast. During March 2005, the shape and magnitude of the poleward flow were similar to those observed during the relaxation season. Still, weak equatorward velocities extended

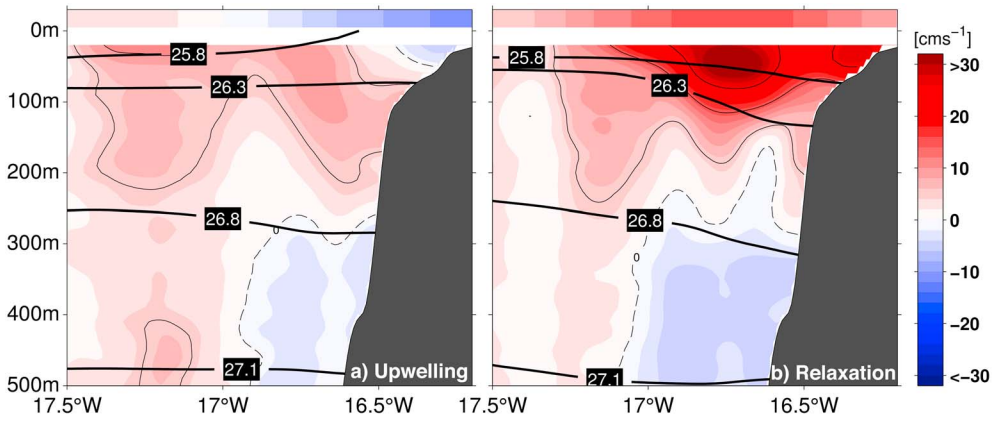

Figure 5. Seasonal mean alongshore velocities (positive poleward, cm/s) as a function of longitude and depth at 18°N for upwelling (December to April) (a) and relaxation (May to July) (b) seasons. Thick black contours depict potential density surfaces, and averaged geostrophic surface velocities from altimetry are indicated in the top of each panel as detailed in Figure 4.

over parts of the shelf, corresponding to upward sloping isopycnals and a poleward flow displaced away from the shelf.

Equatorward flow prevailed throughout the lCW layer between about 250- and 500-m depth in most of the sections with the exception of those taken during March 2005 and June 2014, where little to no equatorward flow in this layer was observed. This deep equatorward flow was particularly enhanced during periods of strong poleward flow in the uCW layer above as depicted in the sections taken in July 2006 and June 2009. During both periods, equatorward flow of about 20 cm/s was distinctly separated from poleward flow in the uCW layer. Away from the boundary current regime, that is, more than 60 km from the shelf break, flow patterns were likely dominated by the effect of mesoscale eddies.

Geostrophic surface velocities determined from satellite altimetry often match the flow patterns observed with the uppermost reliable shipboard ADCP measurements (Figure 4). These data additionally underline the seasonal flow patterns observed in the ship sections. In the velocity sections collected during the upwelling season, equatorward velocities dominated over the shelf. Instead, during the relaxation season, velocities over the shelf were poleward while the poleward flow in the uCW layer was enhanced.

Table 3
Transport Estimates ([Sv]) During Individual Observation Periods and for Relaxation (May to July) and Upwelling (December to April) Seasons at 18°N From Vessel-Mounted Acoustic Doppler Current Profiler Measurements

	Transport [Sv]	
Date	20–250 m	250–500 m
Mar–Apr 2005	1.71	0.55
Jul–Aug 2006	1.50	−0.92
Jan–Feb 2007	0.66	−0.12
Feb 2007	−0.30	−0.18
Feb 2008	0.21	−0.56
Jun 2009	1.92	−0.82
Mar–Apr 2011	1.13	0.10
Jun 2014	1.84	−0.07
Aug 2016	−0.15	−0.80
Relaxation mean	1.75 ± 0.13	−0.60 ± 0.27
Upwelling mean	0.68 ± 0.35	−0.04 ± 0.18

Note. Transports were calculated between 20 and 250 m and 250 and 500 m (corresponding approximately to Tropical Surface Water + upper and lower Central Water layers, respectively), and standard errors for the means are given.

The seasonal mean sections highlight the seasonal differences in the boundary circulation at 18°N (Figure 5). During the relaxation season, elevated poleward flow in excess of 25 cm/s confined to the TSW and uCW layers was observed. Poleward flow during the upwelling season was weak (less than 15 cm/s) and situated above the upper continental slope between 100- and 200-m depth, while on the shelf equatorward flow prevailed. This equatorward flow acted to displace the poleward current farther offshore. Additionally, equatorward flow below 250 m east of 17°W is a distinct feature during both seasons. As indicated in the mean sections, a separation of the deep equatorward flow to the poleward flow above is the 26.8 kg/m^3 isopycnal indicating opposing flows in the lCW and uCW layers. The deep equatorward flow was stronger during the relaxation season but did not exceed 10 cm/s.

Alongshore transports for each velocity section at 18°N were calculated as described in section 2.1. Due to the opposite flow in the TSW and uCW layers with regard to the lCW layer that is apparent in the seasonal mean sections (Figure 5), total transports for these layers were calculated separately (Table 3). The mean poleward transport between 20 and 250 m (corresponding approximately to TSW and uCW layers) during the relaxation season exceeded that during the upwelling season by more

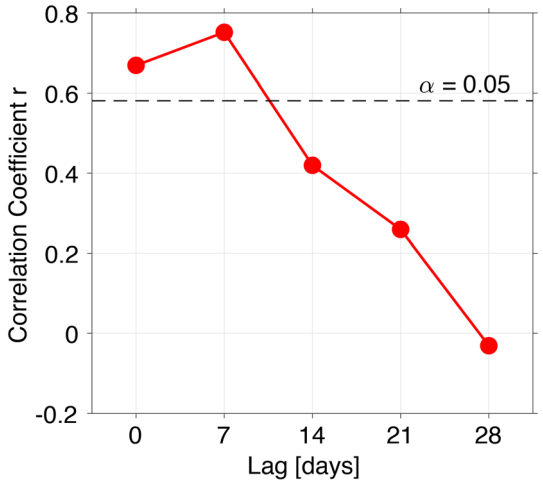

Figure 6. Linear correlation of alongshore transport determined from the individual ship sections (see section 2.1) and Sverdrup transport calculated from weekly averages of the scatterometer winds (see section 2.2) recorded during the respective observational period or leading in time by 7, 14, 21, or 28 days. The dashed line indicates the 95% confidence level ($\alpha = 0.05$).

than a factor of 2.5. Equatorward transport between 250 and 500 m (corresponding approximately to the lCW layer) during the relaxation season was also enhanced compared to the upwelling season.

In summary, the individual velocity sections exhibit elevated current variability but exhibit common seasonal velocity patterns that are reflected in seasonally averaged sections (Figure 5). During the relaxation season, when alongshore winds are weak but wind stress curl is elevated, the average alongshore circulation exhibits a pronounced poleward flow extending from 250 m to the surface. During the upwelling season, when equatorward alongshore wind stress is elevated but wind stress curl is weak, weak poleward flow is observed below a coastal equatorward surface jet. Below 250 m depth, equatorward flow is found during both seasons.

3.2. Transport Variability and Wind Stress Curl

Alongshore transport variability at the eastern boundary can be forced locally by variability of Ekman divergence through CTWs (McCreary, 1981; Suginohara, 1982; Wang, 1982) and offshore propagating Rossby waves (e.g., McCreary & Chao, 1985; Suginohara & Kitamura, 1984) or remotely by CTWs propagating into the region from the South (e.g., Kounta et al., 2018). While locally forced barotropic Rossby waves and barotropic and low-vertical mode baroclinic CTWs can establish an alongshore pressure gradient and related poleward flow at the boundary within a few days, geostrophic adjustment by baroclinic Rossby waves requires several months or more.

To elucidate the driving mechanism of alongshore transport variability at the eastern boundary, a linear correlation between wind stress curl in the form of Sverdrup transport and the transport estimates from the individual cruises (Table 3) was determined for different time lags. Sverdrup transport was calculated from 7-day averages of scatterometer-derived wind stress curl from the coast to 60 km offshore at 18°N observed while the individual velocity section were taken from 7-day averaged wind data collected at different time lags prior to or after these periods. These Sverdrup transports were correlated to the nine transport estimates from the velocity sections between 20 and 500 m (corresponding approximately to TSW, uCW, and lCW layers; see Figures 4 and 5) listed in Table 3. A statistically significant correlation at the 95% ($\alpha = 0.05$) confidence level was found for time lags of zero and 7 days prior to the individual velocity observations (Figure 6). For longer timescales, the correlation rapidly decreases. Similarly, correlations for transport from the velocity sections leading wind stress curl were small and insignificant (not shown). The rapid adjustment of the boundary current transport to wind stress curl variability implies that transport variability along the eastern boundary at 18°N is predominately driven by a fast response of locally forced waves.

Based on these findings, we integrated weekly averaged wind stress curl from 7 days prior to the different section occupations westward from the first available satellite grid point to obtain the stream function $\phi = -\frac{1}{\beta\rho_0}\int_{x_E}^{x} \hat{k}\cdot(\nabla\times\tau)\,dx$, where β is the meridional variation in the coriolis parameter, ρ_0 is a reference density, and $\hat{k}\cdot(\nabla\times\tau)$ is the vertical component of the wind stress curl. Corresponding alongshore velocities between 20 and 500 m were also integrated from the first available grid point of satellite wind data to ensure comparability of our results. Both were then averaged into their respective seasonal means, and their standard error was determined.

Within the boundary current regime eastward of 17.5°W, the average wind-derived and velocity-derived stream functions generally agree during both the relaxation and the upwelling seasons (Figure 7). During both seasons, Sverdrup transport accounts for a large fraction of the observed transport. When including meridional velocities extrapolated to satellite geostrophic surface velocities in the transport calculations, results are not significantly altered. Similarly, mean meridional Ekman transport in the surface layer across 18°N between 16°W and 17°W not considered in the observed transports was low, that is, 2.2×10^{-2} and -6.6×10^{-2} Sv during the respective seasons and thus does not affect the above result.

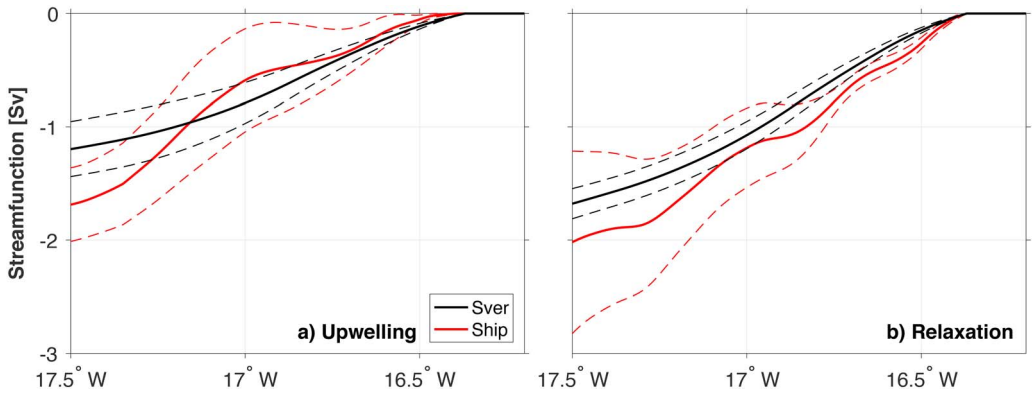

Figure 7. Stream functions ([Sv]) of Sverdrup transport and ship-based transports between 20- and 500-m water depth integrated westward from the first available satellite grid point as a function of longitude for upwelling (December to April) (a) and relaxation (May to July) (b) seasons. Thin dashed lines indicate the standard errors.

The close agreement of the observed transport stream function and Sverdrup stream function determined from wind stress curl 7 days prior to the velocity observations requires that within 60 km of the eastern boundary, wave processes must establish large parts of the geostrophic adjustment on short timescales. Again, this suggests a dominant role of locally forced waves in controlling the eastern boundary current transport off Mauritania.

3.3. Hydrography and Oxygen

During the upwelling season, lower upper-ocean temperatures of about 15 °C prevailed on the shelf (Figure 8a). Active wind-driven upwelling was indicated by the shallowing of the 25.8 kg/m^3 isopycnal toward

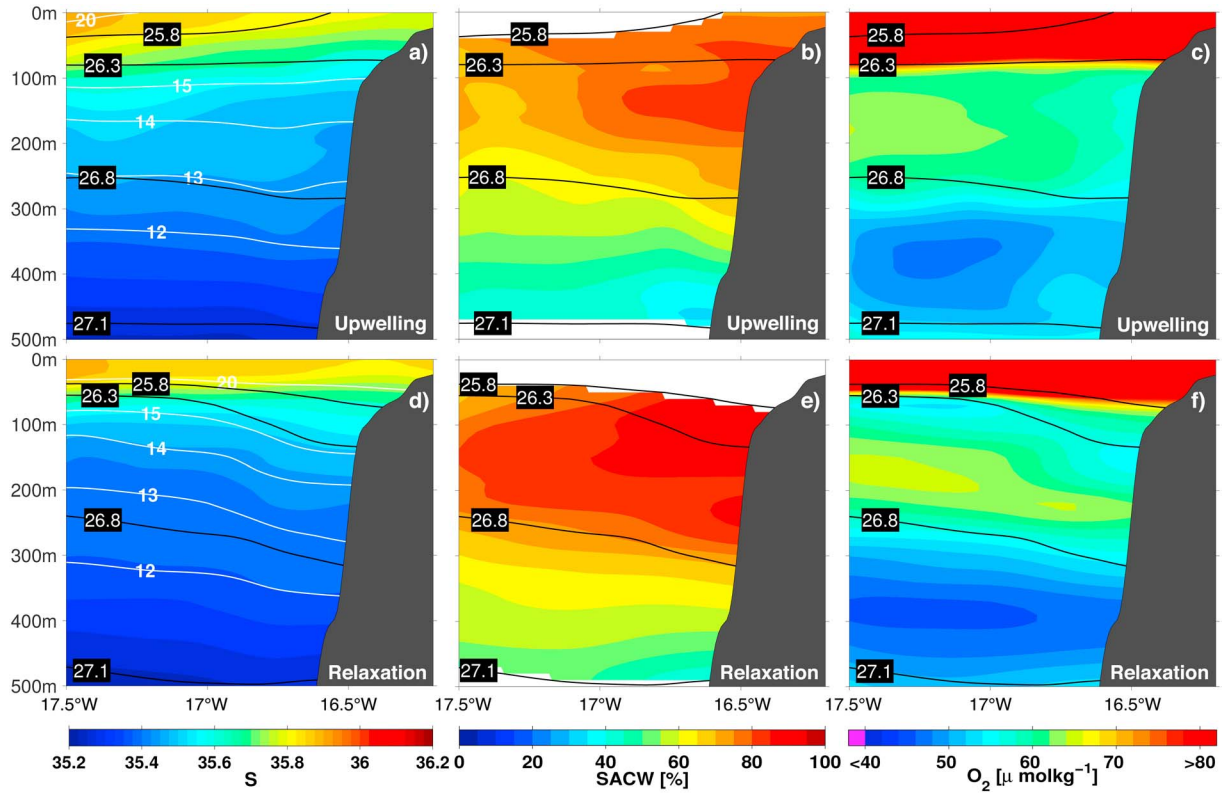

Figure 8. Seasonal mean salinity (color) and temperature (white contours, °C) (a, d), South Atlantic Central Water (SACW) concentrations (b, e), and oxygen concentrations (μmol/kg, c, f) as a function of longitude and depth at 18°N for upwelling (December to April; top) and relaxation (May to July; bottom) seasons. Black contours in all panels depict potential density surfaces.

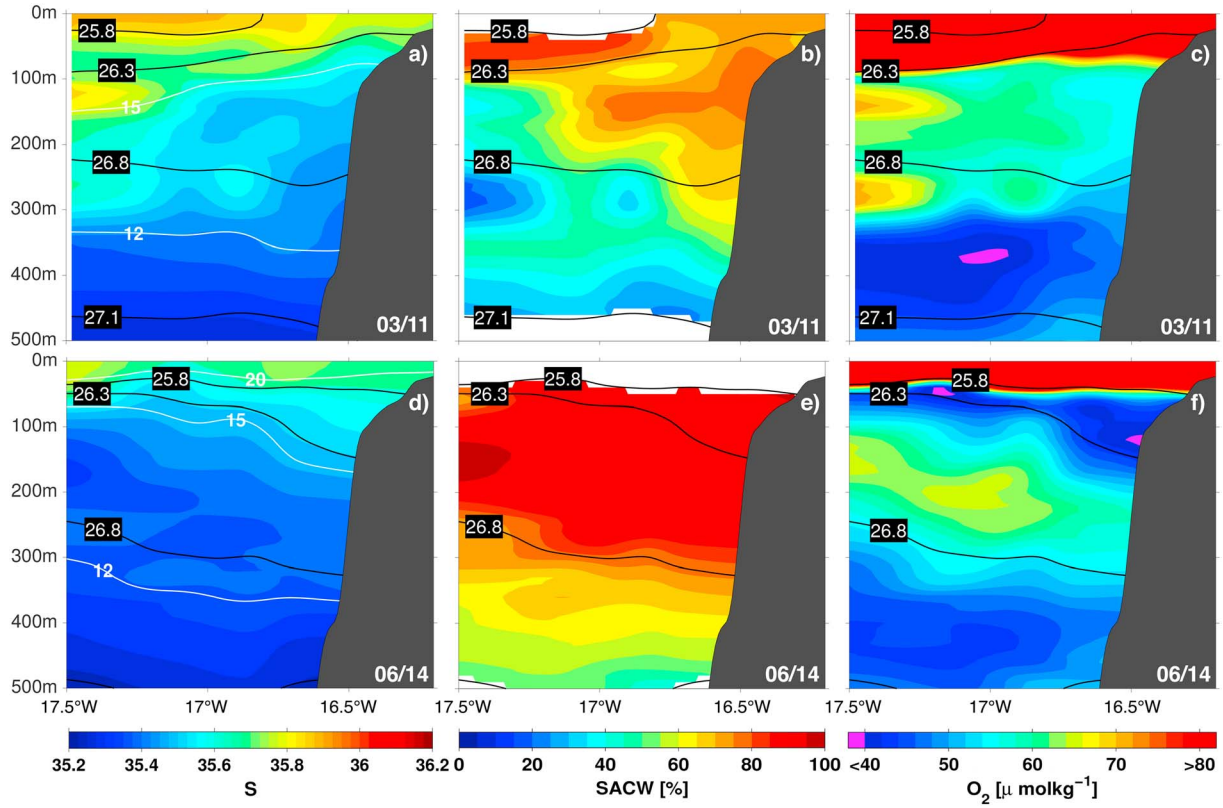

Figure 9. Same as Figure 8 but showing individual cruises MSM17/4 during March 2011 (top) and M107 during June 2014 (bottom). SACW = South Atlantic Central Water.

the coast with outcropping of that isopycnal at about 16.6°W (Figure 8a). Hydrography during the relaxation season was characterized by higher temperatures above 20 °C and high salinities in the surface layer (Figure 8d). In the uCW layer, lower salinity waters were present during the relaxation season compared to the upwelling season. Individual hydrographic sections occasionally showed particularly low salinities in the uCW layer, for example, during June 2014 (Figure 9d). The central water layer is prone to intrusions of waters of higher/lower salinities compared to its surrounding waters due to the distinct differences of NACW and SACW properties. Intrusions of lower salinity waters were observed during the upwelling season as shown close to the continental slope in Figure 9a compiled from March 2011 data. Examples of high salinity intrusions are clearly visible in the uCW layer (just below the 26.3-kg/m^3 isopycnal) during March 2011 (Figure 9a).

The overall freshening observed in the uCW layer from the upwelling to the relaxation season coincided with a cooling in that layer (Figures 8a and 8d), as indicated by the shoaling of the 13 and 14 °C isotherms.

SACW concentrations calculated from temperature and salinity measurements underline the seasonal variability of water masses within the central water stratum (Figures 8b, 8e, 9b, and 9e). Central waters consisted of around 70–80% SACW throughout most of the uCW layer during the upwelling season and exceeded 80–90% SACW close to the continental slope during the relaxation season (Figure 8e). In contrary, SACW contributed less than 50% to the water masses in the lCW layer. The change in SACW concentrations from the uCW to the lCW layers was reflected in the water mass analysis from all individual cruises. Conversely, observed water mass compositions in the individual cruise data often reflected the prevailing velocity structure. For example, enhanced SACW concentrations in the vicinity of the continental slope at depths between 100 and 250 m during March 2011 closely resembled the shape and vertical extent of the poleward flow observed during that cruise (Figures 4 and 9b).

Oxygen concentrations generally decreased from the uCW layer to the lCW layer in all of the cruises in our data set, independent of season (Figures 8c and 8f). During two relaxation season cruises, however, a

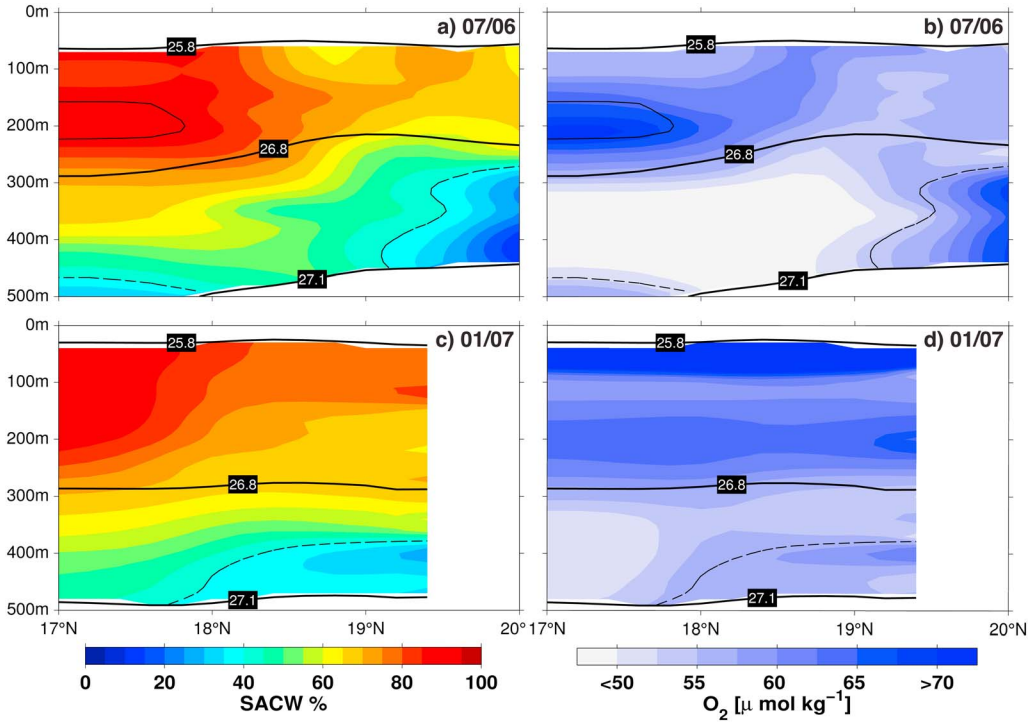

Figure 10. South Atlantic Central Water (SACW) concentration (a, c) and oxygen concentration (b, d) (in μmol/kg) as a function of latitude and depth averaged between the coast and 200 km offshore during cruises M68/3 in July 2006 (top) and P347 in January 2007 (bottom). Thick black contours depict potential density surfaces, and thin solid and dashed contours indicate 90% and 40% isolines of SACW concentration, respectively.

distinct local oxygen minimum situated at about the 26.3 kg/m^3 isopycnal was observed, with lowest oxygen concentrations at the shelf break around 100-m water depth (Figure 9f for June 2014).

3.4. Meridional Sections

The northward penetration of SACW in the boundary currents in the uCW layer as well as the southward penetration of NACW in the lCW was analyzed using alongshore sections of SACW and oxygen concentrations taken during July 2006 and January 2007. These cruises were chosen, because they provided the most extensive spatial coverage and were the only two cruises in the data set that were conducted in successive relaxation/upwelling seasons. Available CTD-O_2 stations between 17°N to 20°N were averaged to include all measurements within the central water stratum and 200 km from the coast.

The southward intrusions of waters consisting of predominantly NACW in the lCW layer and the northward penetration of SACW in the uCW layer reflect the opposing boundary flows in the respective layers during both cruises. In general, oxygen decreases downstream in both layers, that is, poleward in the uCW layer and equatorward in the lCW layer. Enhanced oxygen concentrations are found for SACW concentrations larger than 90% and smaller than 40% in the uCW and lCW layers, respectively (Figures 10b and 10d). This relationship between water mass and oxygen concentration in the central water stratum was invariant between cruises performed during upwelling and relaxation seasons. Layer thicknesses of the central water layers covaried such that a thin uCW layer coincided with a thicker lCW layer and vice versa.

4. Discussion

The main focus of this study was a description of the seasonal variability of the EBC in the MUR on the basis of nine research cruises conducted between 2005 and 2016. The combination of velocity, hydrographic, and oxygen data provided the opportunity to assess the seasonal variability in the distribution of the central water masses, their renewal, and associated ventilation in the MUR.

The individual ship sections showed enhanced poleward flow in the TSW and uCW layers at 18°N during the relaxation season in comparison to the upwelling season. These conditions reflect the seasonal intensification and surfacing of the MC, extending over the continental shelf and slope and coinciding with a rapid warming of near-coastal SSTs in the region to about 20°N during that season (Lathuilière et al., 2008). The shape, structure, and magnitude of the observed flow generally agree with previous observations based on individual cruises by Mittelstaedt (1983) and Peña-Izquierdo et al. (2012). Peña-Izquierdo et al. (2012) reported poleward transports on the order of 2.4 Sv at 17.75°N in the TSW and uCW layers based on direct velocity observations during a cruise conducted in November 2008. The magnitude of their poleward transport from that season is thus somewhat larger than the poleward transports during upwelling and relaxation season of 0.7 and 1.8 Sv, respectively, reported here. ROMS by Kounta et al. (2018) suggested elevated poleward transports at the eastern boundary during the boreal fall season due to CTWs excited in the Gulf of Guinea, which may explain this discrepancy.

The upwelling season exhibited less intense poleward flow that was found attached to the slope and shelf break between 100- and 200-m depth. On the shelf, in the near surface layer, equatorward flow was present in most of the sections collected during the upwelling season. As suggested by modeling and theoretical studies, the relative strength of the equatorward surface jet and the PUC depends on the relative strength of wind stress and wind stress curl, particularly near the coast (e.g., Capet et al., 2004; Fennel et al., 2012; McCrearyet al., 1987). During the upwelling season, when the wind stress curl near the coast is reduced (Figure 7), the current system exhibits an equatorward surface jet as is predicted by theory in response to equatorward wind. This gives the MC the appearance of an undercurrent during the upwelling season. Elevated wind stress curl near the coast during the relaxation season allows the undercurrent to reach the sea surface, and the equatorward surface jet weakens or vanishes.

The flow in the lCW layer between about 250 and 500 m was predominantly equatorward at about 10 cm/s. It intensified during the relaxation season. The observed opposing flow regimes in the two central water layers compare well with the results obtained by Peña-Izquierdo et al. (2015) who suggested by analyzing hydrographic data and the output of an assimilation model opposing circulation cells in the upper and lCW layers. Equatorward flow below the poleward eastern boundary currents was also observed in the upwelling region off Peru (e.g., Chaigneau et al., 2013) and off Angola (Tchipalanga et al., 2018), suggesting that it is a common feature of EBC. Our data show stronger equatorward flow during the relaxation season compared to the upwelling season in that depth range, pointing to a baroclinic response of the circulation to the wind stress curl as a driving mechanism.

A somewhat unexpected result was the finding of a rapid adjustment of the boundary current transport to wind stress curl variability. Significant (95%) correlation between wind stress curl and alongshore transport was found for time lags of zero and 7 days prior to the individual velocity observations. At longer time scales, the correlation rapidly decreases. Besides barotropic Rossby waves, a possible explanation of the short time lag is that the ocean adjustment to the wind stress curl at the eastern boundary occurs through locally forced CTWs. The first four baroclinic mode CTWs exhibit phase velocities between 4 and 5 m/s (first mode) and 0.6 and 0.9 m/s (fourth mode) depending predominately on the steepness of the continental slope (e.g., Illig et al., 2018). Thus, baroclinic alongshore pressure gradients can be set up rather rapidly for a limited stretch of coastline. The rapid decrease of the correlation at longer time scale may be associated with elevated high-frequency wind variability encountered at the eastern boundary. Mittelstaedt (1983) reported elevated wind stress variability on timescales of 5 to 10 days. Similarly, Lathuilière et al. (2008) were able to attribute intermittent periods of phytoplankton growth to short-term variations of alongshore wind stress.

Enhanced mesoscale activity in the MUR is well documented. Schütte et al. (2016) showed that the generation of anticyclonic as well as cyclonic eddies at the eastern boundary seasonally peaks between May and July. Thus, we assume that particularly during the relaxation season, the adjustment of the EBC to the winds is superimposed by mesoscale activity contributing to variability of alongshore transport observed in our sections.

From our water mass analysis, we have shown that the vertical change in central water characteristics from predominantly SACW in the uCW layer to a mixture of SACW and NACW in the lCW layer was observed during all cruises presented in this study, indicating a seasonally independent behavior. The transition occurred at around the 26.8-kg/m^3 isopycnal, coinciding with the boundary of upper and lCWs as well as opposing

poleward and equatorward flows observed in these layers. The high SACW concentrations in the uCW layer indicate a more direct pathway into the MUR from the Southern Hemisphere. Oxygen generally decreases downstream the main flow, that is, poleward in the uCW layer and equatorward in the lCW layer. The transition to less oxygenated waters at the same isopycnal is found to be associated with a change in water mass composition throughout all cruises presented here. Meridional sections taken during two successive upwelling/relaxation cruises further suggest that ventilation of the uCW and lCW layers occurs from the south and north, respectively. This has previously been proposed through modeling studies by Elmoussaoui et al. (2005) and Peña-Izquierdo et al. (2015) and was inferred from observed hydrographic properties and oxygen distributions by Voituriez and Chuchla (1978). Waters high in SACW concentration advected from the south in the uCW layer, and waters high in NACW concentration from the north in the lCW layer were both higher in oxygen concentrations with respect to ambient waters. This suggests the existence of a northerly ventilation pathway in the lCW layer in the MUR, having potential implications for the ventilation of the oxygen minimum zone of the tropical North Atlantic (e.g., Brandt et al., 2015). Pastor et al. (2012) attributed higher oxygen concentrations in water masses exhibiting high NACW concentrations to their more recent subduction in the subtropical gyre of the North Atlantic.

The lower potential density boundary of the uCW is likely connected to the vertical extent of the eastward flowing North Equatorial Undercurrent (NEUC) and North Equatorial Countercurrent (NECC) transporting Southern Hemisphere waters eastward. Using lowered ADCP measurements along 35°W, Schott et al. (2003) found the lower boundary of waters carried within the NEUC to be around the 26.8-kg/m^3 isopycnal. This was validated for both the NEUC and the NECC by Elmoussaoui et al. (2005) through model simulations. Further, Brandt et al. (2015) showed that the eastward flow in the northern branch of the NECC (nNECC) at about 8°N and 23°W above the 26.8 kg/m^3 isopycnal was similarly strong compared to the NEUC. Taking into account the water mass distribution in the western tropical North Atlantic as outlined by Kirchner et al. (2009), the nNECC likely contributes to the ventilation of the uCW layer.

Despite the advection of SACW in the uCW that is particularly evident during the relaxation season, very low oxygen concentrations close to the shelf break at 18°N were observed during two relaxation season cruises. These low oxygen concentrations could be related to weaker diapycnal oxygen fluxes during that season. Diapycnal oxygen fluxes above 500 m water depth in the region were reported to exceed the benthic oxygen uptake by a factor of about seven during two upwelling cruises (Brandt et al., 2015). Due to stronger stratification over the continental slope and shelf however, the diapycnal supply of oxygen from the surface into the seasonally stratified ocean would be greatly reduced during the relaxation season. Benthic oxygen uptake was found to exhibit almost no seasonal variability by Dale et al. (2014) and to be as high as 10 mmol·m^{-2}·day^{-1} for water depths from 50 to 100 m, which coincides with regions of extremely low oxygen concentrations observed during June 2014 and August 2016. In the absence of diapycnal oxygen supply from the well-ventilated surface layer, these fluxes in combination with prolonged periods of respiration in the wake of the upwelling season (Lathuilière et al., 2008) could explain the low oxygen concentrations observed during the relaxation season cruises.

5. Conclusion

Our multicruise data set provides observational evidence for the relative contributions of alongshore wind stress and wind stress curl to the boundary current flow structure. During the upwelling season, when alongshore wind stress is at its maximum but wind stress curl is weak, equatorward flow dominates on the shelf, and the poleward MC has the appearance of an undercurrent of 30–40-km width with maximum average velocities of about 10 cm/s at 100-m water depth and a transport of 0.7 Sv. During the relaxation season between May and July, a strengthened MC extends from the surface throughout the uCW layer, flowing against the local winds and transporting waters of mainly South Atlantic origin into the MUR. The mean MC transport between 20 and 250 m was 1.75 Sv, 2.5 times larger compared to the upwelling season. During this period, wind stress curl is at its maximum while alongshore wind stress is weak, coinciding with an offshore displacement of the zero-wind stress curl contour. These results underline the importance of the precise cross-shore wind structure for correctly simulating the EBC in upwelling regions that has been suggested previously (Fennel et al., 2012; Harlaß et al., 2015, 2018; Junker et al., 2015; McCreary & Chao, 1985; Patricola &

Chang, 2017; Small et al., 2015). Underneath the MC in the lCW layer, average flow was equatorward during both seasons.

The rapid adjustment of the boundary current transport to wind stress curl variability implies that transport variability along the eastern boundary at 18°N is predominately driven by locally forced waves. Similarly, the close agreement of the observed transport stream function and Sverdrup stream function determined from wind stress curl 7 days prior to the velocity observations requires that within 60 km of the eastern boundary, wave processes must establish large parts of the geostrophic adjustment on short timescales.

The renewal of water masses in the uCW layer occurs mainly during the relaxation season, suggested by the large amounts of SACW observed during that time. A possible northerly advection pathway of oxygenated NACW in the lCW layer could be identified, with likely implications for the ventilation of the North Atlantic oxygen minimum zone.

Acknowledgments
This study was supported by the Deutsche Forschungsgemeinschaft as part of the Sonderforschungsbereich 754 "Climate—Biogeochemistry Interactions in the Tropical Ocean" (www.sfb754.de). It was further supported by the European Union 7th Framework Programme (FP7 2007–2013) under grant agreement 603521 PREFACE project. The authors would like to sincerely thank all captains and crews of the respective research vessels, as well as all PIs, scientists, and students involved in the various projects and research cruises used in this study. Data sets described in section 2.1 are available through the world data center PANGAEA at https://doi.org/10.1594/PANGAEA: 817235 (CTD, P320), 667374 (VM-ADCP, P320), 771866 (CTD, P347), 704433 (VM-ADCP, P347), 848597 (CTD, P348), 854808 (VM-ADCP, P348), 787808 (CTD, M68/3), 853930 (CTD, ATA3), 848614 (CTD, P399), 854848 (VM-ADCP, P399), and doi registration for cruises MSM17/4, M107, and M129 and for data sets (VM-ADCP, M68/3) and (VM-ADCP, ATA3) in progress. QuikSCAT data are produced by remote sensing systems and sponsored by the NASA Ocean Vector Winds Science Team. Data are available at www.remss.com. C-2015 ASCAT data are produced by remote sensing systems and sponsored by the NASA Ocean Vector Winds Science Team. Data are available at www.remss.com. Furthermore, the study was conducted using E.U. Copernicus Marine Service Information by accessing altimetry data available at http://marine.copernicus.eu/. The authors would like to thank two anonymous reviewers for their helpful comments.

References

Bange, H. W. (2008). FS Poseidon Fahrtbericht/Cruise Report P348, SOPRAN: Mauritanian Upwelling Study 2007. *Berichte Aus Dem Leibniz-Institut Für Meereswissenschaften an Der Christian-Albrechts-Universität Zu Kiel*, *18*, 1–36. https://doi.org/10.3289/ifm-geomar_rep_18_2008

Bange, H. W. (2011). FS POSEIDON Fahrtbericht/Cruise Report P399 - 2&3. *Berichte Aus Dem Leibniz-Institut Für Meereswissenschaften an Der Christian-Albrechts-Universität Zu Kiel*, *48*, 1–84. https://doi.org/10.3289/ifm-geomar_rep_48_2011

Barton, E. D. (1989). The poleward undercurrent on the eastern boundary of the subtropical North Atlantic. In *Poleward flows along eastern boundaries*, (Vol. 34, pp. 82–95). New York: Springer.

Barton, E. D., Aristegui, J., Tett, P., Canton, M., García-Braun, J., Hernández-León, S., et al. (1998). The transition zone of the canary current upwelling region. *Progress in Oceanography*, *41*(4), 455–504. https://doi.org/10.1016/S0079-6611(98)00023-8

Brandt, P., Bange, H. W., Banyte, D., Dengler, M., Didwischus, S. H., Fischer, T., et al. (2015). On the role of circulation and mixing in the ventilation of oxygen minimum zones with a focus on the eastern tropical North Atlantic. *Biogeosciences*, *12*(2), 489–512. https://doi.org/10.5194/bg-12-489-2015

Brink, K. H., Halpern, D., Huyer, A., & Smith, R. L. (1983). The physical environment of the Peruvian upwelling system. *Progress in Oceanography*, *12*(3), 285–305. https://doi.org/10.1016/0079-6611(83)90011-3

Capet, X. J., Marchesiello, P., & McWilliams, J. C. (2004). Upwelling response to coastal wind profiles. *Geophysical Research Letters*, *31*, L13311. https://doi.org/10.1029/2004GL020123

Chaigneau, A., Dominguez, N., Eldin, G., Vasquez, L., Flores, R., Grados, C., & Echevin, V. (2013). Near-coastal circulation in the northern Humboldt Current System from shipboard ADCP data. *Journal of Geophysical Research: Oceans*, *118*, 5251–5266. https://doi.org/10.1002/jgrc.20328

Dale, A. W., Sommer, S., Ryabenko, E., Noffke, A., Bohlen, L., Wallmann, K., et al. (2014). Benthic nitrogen fluxes and fractionation of nitrate in the Mauritanian oxygen minimum zone (eastern tropical North Atlantic). *Geochimica et Cosmochimica Acta*, *134*, 234–256. https://doi.org/10.1016/j.gca.2014.02.026

Dengler, M., Schafstall, J., Tanhua, T., Fiedler, B., Krahmann, G., & Löptien, U. (2008). FS Poseidon Fahrtbericht/Cruise Report P347, Mauritanian Upwelling and Mixing Process Study (MUMP). *Berichte Aus Dem Leibniz-Institut Für Meereswissenschaften an Der Christian-Albrechts-Universität Zu Kiel*, *16*, 1–34. https://doi.org/10.3289/ifm-geomar_rep_16_2008

Ekau, W., Bachmann, J., Bahlman, E., Balde, B., Börner, G., Bröhl, S., et al. (2016). The role of the Banc d'Arguin and Sine Saloum as sink for matter fluxes and source for productivity of the southern Canary Current, BASS, Cruise No. M129. In *METEOR-Berichte*. DFG-Senatskommission für Ozeanographie.

Elmoussaoui, A., Arhan, M., & Treguier, A. M. (2005). Model-inferred upper ocean circulation in the eastern tropics of the North Atlantic. *Deep-Sea Research Part I: Oceanographic Research Papers*, *52*(7), 1093–1120. https://doi.org/10.1016/j.dsr.2005.01.010

Fennel, W. (1999). Theory of the Benguela upwelling system. *Journal of Physical Oceanography*, *29*(2), 177–190. https://doi.org/10.1175/1520-0485(1999)029<0177:TOTBUS>2.0.CO;2

Fennel, W., Junker, T., Schmidt, M., & Mohrholz, V. (2012). Response of the Benguela upwelling systems to spatial variations in the wind stress. *Continental Shelf Research*, *45*, 65–77. https://doi.org/10.1016/j.csr.2012.06.004

Fischer, T., Banyte, D., Brandt, P., Dengler, M., Krahmann, G., Tanhua, T., & Visbeck, M. (2013). Diapycnal oxygen supply to the tropical North Atlantic oxygen minimum zone. *Biogeosciences*, *10*(7), 5079–5093. https://doi.org/10.5194/bg-10-5079-2013

Glessmer, M. S., Eden, C., & Oschlies, A. (2009). Contribution of oxygen minimum zone waters to the coastal upwelling off Mauritania. *Progress in Oceanography*, *83*(1–4), 143–150. https://doi.org/10.1016/j.pocean.2009.07.015

Harlaß, J., Latif, M., & Park, W. (2015). Enhanced vertical atmosphere resolution improves climate model simulation of tropical Atlantic sea surface temperature and interannual variability. *Geophysical Research Letters*, *42*, 2401–2408. https://doi.org/10.1002/2015GL063310

Harlaß, J., Latif, M., & Park, W. (2018). Alleviating tropical Atlantic sector biases in the Kiel climate model by enhancing horizontal and vertical atmosphere model resolution: climatology and interannual variability. *Climate Dynamics*, *50*, 2605–2635. https://doi.org/10.1007/s00382-017-3760-4

Illig, S., Cadier, E., Bachèlery, M.-L., & Kersalé, M. (2018). Subseasonal coastal-trapped wave propagations in the southeastern Pacific and Atlantic Oceans: 1. A new approach to estimate wave amplitude. *Journal of Geophysical Research: Oceans*, *123*, 3915–3941. https://doi.org/10.1029/2017JC013539

Johns, W. E., Zantopp, R. J., & Goni, G. J. (2003). Cross-gyre transport by North Brazil Current rings. *Elsevier Oceanography Series*, *68*, 411–441. https://doi.org/10.1016/S0422-9894(03)80156-3

Junker, T., Schmidt, M., & Mohrholz, V. (2015). The relation of wind stress curl and meridional transport in the Benguela upwelling system. *Journal of Marine Systems*, *143*, 1–6. https://doi.org/10.1016/j.jmarsys.2014.10.006

Kirchner, K., Rhein, M., Hüttl-Kabus, S., & Böning, C. W. (2009). On the spreading of South Atlantic water into the northern hemisphere. *Journal of Geophysical Research*, *114*, C05019. https://doi.org/10.1029/2008JC005165

Kopte, R., Brandt, P., Claus, M., Greatbatch, R. J., & Dengler, M. (2018). Role of Equatorial Basin-mode resonance for the seasonal variability of the Angola current at 11°S. *Journal of Physical Oceanography*, *48*(2), 261–281. https://doi.org/10.1175/JPO-D-17-0111.1

Körtzinger, A. (2008). Short Cruise Report R/V L'Atalante Cruise IFM-GEOMAR, leg 3.
Koschinsky, A., Brandt, P., & Körtzinger, A. (2009). Tropical Atlantic 2006, Cruise No. 68, April 26 - August 7, 2006. *METEOR-Berichte*, *M68*, 1–188. https://doi.org/10.2312/cr_m68
Kounta, L., Capet, X., Jouanno, J., Kolodziejczyk, N., Sow, B., & Gaye, A. T. (2018). A model perspective on the dynamics of the shadow zone of the eastern tropical North Atlantic. Part 1: The poleward slope currents along West Africa. *Ocean Science*, *14*(5), 971–997. https://doi.org/10.5194/os-14-971-2018
Large, W. G., & Pond, S. (1981). Open Ocean momentum flux measurements in moderate to strong winds. *Journal of Physical Oceanography*, *11*(3), 324–336. https://doi.org/10.1175/1520-0485(1981)011<0324:OOMFMI>2.0.CO;2
Lathuilière, C., Echevin, V., & Lévy, M. (2008). Seasonal and intraseasonal surface chlorophyll-*a* variability along the northwest African coast. *Journal of Geophysical Research*, *113*, C05007. https://doi.org/10.1029/2007JC004433
Marchesiello, P., McWilliams, J. C., & Shchepetkin, A. (2003). Equilibrium structure and dynamics of the California current system. *Journal of Physical Oceanography*, *33*(4), 753–783. https://doi.org/10.1175/1520-0485(2003)33<753:ESADOT>2.0.CO;2
McCreary, J. P. (1981). A linear stratified Ocean model of the coastal undercurrent. *Philosophical Transactions of the Royal Society of London. Series A, Mathematical and Physical Sciences*, *302*(1469), 385–413. https://doi.org/10.1098/rsta.1981.0176
McCreary, J. P., & Chao, S.-Y. (1985). Three-dimensional shelf circulation along an eastern ocean boundary. *Journal of Marine Research*, *43*(1), 13–36. https://doi.org/10.1357/002224085788437316
McCreary, J. P., Kundu, P. K., & Chao, S.-Y. (1987). On the dynamics of the California current system. *Journal of Marine Research*, *45*(1), 1–32. https://doi.org/10.1357/002224087788400945
Mittelstaedt, E. (1983). The upwelling area off Northwest Africa—A description of phenomena related to coastal upwelling. *Progress in Oceanography*, *12*(3), 307–331. https://doi.org/10.1016/0079-6611(83)90012-5
Mittelstaedt, E. (1991). The ocean boundary along the northwest African coast: Circulaton and oceanographic properties at the sea surface. *Progress in Oceanography*, *26*(4), 307–355. https://doi.org/10.1016/0079-6611(91)90011-A
Mohrholz, V., Eggert, A., Junker, T., Nausch, G., Ohde, T., & Schmidt, M. (2014). Cross shelf hydrographic and hydrochemical conditions and their short term variability at the northern Benguela during a normal upwelling season. *Journal of Marine Systems*, *140*, 92–110. https://doi.org/10.1016/j.jmarsys.2014.04.019
Munk, W. H. (1950). On the wind-driven ocean circulation. *Journal of Meteorology*, *7*(2), 80–93. https://doi.org/10.1175/1520-0469(1950)007<0080:OTWDOC>2.0.CO;2
Pastor, M. V., Peña-Izquierdo, J., Pelegrí, J. L., & Marrero-Díaz, Á. (2012). Meridional changes in water mass distributions off NW Africa during November 2007/2008. *Ciencias Marinas*, *38*(1B), 223–244. https://doi.org/10.7773/cm.v38i1B.1831
Patricola, C. M., & Chang, P. (2017). Structure and dynamics of the Benguela low-level coastal jet. *Climate Dynamics*, *49*(7–8), 2765–2788. https://doi.org/10.1007/s00382-016-3479-7
Peña-Izquierdo, J., Pelegrí, J. L., Pastor, M. V., Castellanos, P., Emelianov, M., Gasser, M., et al. (2012). The continental slope current system between Cape Verde and the Canary Islands. *Scientia Marina*, *76*(S1), 65–78. https://doi.org/10.3989/scimar.03607.18C
Peña-Izquierdo, J., Van Sebille, E., Pelegri, J. L., Sprintall, J., Mason, E., Llanillo, P. J., & Machin, F. (2015). Water mass pathways to the North Atlantic oxygen minimum zone. *Journal of Geophysical Research: Oceans*, *120*, 3350–3372. https://doi.org/10.1002/2014JC010557
Pfannkuche, O. (2014). Climate-Biogeochemistry interactions in the tropical ocean of the NW-African oxygen minimum zone (SFB754) - Cruise No. MSM17/4 - March 10 - April 11, 2011 - Dakar (Senegal) - Las Palmas (Spain). *MARIA S. MERIAN-Berichte, MSM17/4*, 1–59. https://doi.org/10.2312/cr_msm17_4
Philander, S. G. H., & Yoon, J.-H. (1982). Eastern boundary currents and coastal upwelling. *Journal of Physical Oceanography*, *12*(8), 862–879. https://doi.org/10.1175/1520-0485(1982)012<0862:EBCACU>2.0.CO;2
Polo, I., Lazar, A., Rodriguez-Fonseca, B., & Arnault, S. (2008). Oceanic Kelvin waves and tropical Atlantic intraseasonal variability: 1. Kelvin wave characterization. *Journal of Geophysical Research*, *113*, C07009. https://doi.org/10.1029/2007JC004495
Risien, C. M., & Chelton, D. B. (2008). A global climatology of surface wind and wind stress fields from eight years of QuikSCAT Scatterometer data. *Journal of Physical Oceanography*, *38*(11), 2379–2413. https://doi.org/10.1175/2008JPO3881.1
Ruhland, G., Alamo, N., Barrera, C., Dehning, K., Klar, S., Koester, J. J., et al. (2005). Report and preliminary results of Poseidon Cruise 320, Las Palmas—Las Palmas, 08.03–18.03.2005. In *Berichte, Fachbereich Geowissenschaften*. Universität Bremen.
Schott, F. A., Dengler, M., Brandt, P., Affler, K., Fischer, J., Bourlès, B., et al. (2003). The zonal currents and transports at 35°W in the tropical Atlantic. *Geophysical Research Letters*, *30*(7), 1349. https://doi.org/10.1029/2002GL016849
Schütte, F., Brandt, P., & Karstensen, J. (2016). Occurrence and characteristics of mesoscale eddies in the tropical northeastern Atlantic Ocean. *Ocean Science*, *12*(3), 663–685. https://doi.org/10.5194/os-12-663-2016
Small, R. J., Curchitser, E., Hedstrom, K., Kauffman, B., & Large, W. G. (2015). The Benguela upwelling system: Quantifying the sensitivity to resolution and coastal wind representation in a global climate model. *Journal of Climate*, *28*(23), 9409–9432. https://doi.org/10.1175/JCLI-D-15-0192.1
Sommer, S., Dengler, M., & Treude, T. (2015). Benthic element cycling, fluxes and transport of solutes across the benthic boundary layer in the Mauritanian oxygen minimum zone, (SFB754) - Cruise No. M107 - May 30 - July 03, 2014 - Fortaleza (Brazil) - Las Palmas (Spain). *Meteor-Berichte*, *M107*, 1–54. https://doi.org/10.2312/cr
Stramma, L., Brandt, P., Schafstall, J., Schott, F., Fischer, J., & Körtzinger, A. (2008). Oxygen minimum zone in the North Atlantic south and east of the Cape Verde Islands. *Journal of Geophysical Research*, *113*, C04014. https://doi.org/10.1029/2007JC004369
Stramma, L., Hüttl, S., & Schafstall, J. (2005). Water masses and currents in the upper tropical northeast Atlantic off northwest Africa. *Journal of Geophysical Research*, *110*, C12006. https://doi.org/10.1029/2005JC002939
Suginohara, N. (1982). Coastal upwelling: Onshore-offshore circulation, equatorward coastal jet and poleward undercurrent over a continental shelf-slope. *Journal of Physical Oceanography*, *12*(3), 272–284. https://doi.org/10.1175/1520-0485(1982)012<0272:CUOCEC>2.0.CO;2
Suginohara, N., & Kitamura, Y. (1984). Long-term coastal upwelling over a continental shelf-slope. *Journal of Physical Oceanography*, *14*(6), 1095–1104. https://doi.org/10.1175/1520-0485(1984)014<1095:LTCUOA>2.0.CO;2
Tchipalanga, P., Dengler, M., Brandt, P., Kopte, R., Macuéria, M., Coelho, P., et al. (2018). Eastern boundary circulation and hydrography off Angola—Building Angolan oceanographic capacities. *Bulletin of the American Meteorological Society*, *99*(8), 1589–1605. https://doi.org/10.1175/BAMS-D-17-0197.1.
Van Camp, L., Nykjaer, L., Mittelstaedt, E., & Schlittenhardt, P. (1991). Upwelling and boundary circulation off Northwest Africa as depicted by infrared and visible satellite observations. *Progress in Oceanography*, *26*(4), 357–402. https://doi.org/10.1016/0079-6611(91)90012-B

Voituriez, B., & Chuchla, R. (1978). Influence of the southern Atlantic Central Water on the distribution of salinity and oxygen in the northeast tropical Atlantic Ocean. *Deep-Sea Research*, *25*, 107–117.

Wang, D. P. (1982). Development of a three-dimensional, limited-area (island) shelf circulation model. *Journal of Physical Oceanography*, *12*(7), 605–617. https://doi.org/10.1175/1520-0485(1982)012<0605:DOATDL>2.0.CO;2